INTERFACE

royalsocietypublishing.org/rsif

Research

Cite this article: Roy Chowdhury P, Wang TX, MacDonald A, Tierney K, Wang H. 2026 Pollutant-induced changes in fish pigmentation and spatial patterns. *J. R. Soc. Interface* **23**: 20260065.
https://doi.org/10.1098/rsif.2026.0065

Received: 18 January 2026
Accepted: 29 April 2026

Subject Category:
Life Sciences–Mathematics interface

Subject Areas:
biomathematics, computational biology

Keywords:
hypopigmentation, pattern formation, non-local diffusion–advection, water pollutants, pigment cell interaction

Author for correspondence:
Hao Wang
e-mail: hao8@ualberta.ca

†These authors contributed equally to this study.

Supplementary material is available online at https://doi.org//10.6084/m9.figshare.c.8561734.

THE ROYAL SOCIETY PUBLISHING

Pollutant-induced changes in fish pigmentation and spatial patterns

Pranali Roy Chowdhury[1,4,†], Tian Xu Wang[1,†], Abbey MacDonald[2], Keith Tierney[2,3] and Hao Wang[1]

[1]Department of Mathematical and Statistical Sciences, [2]Department of Biological Sciences and [3]School of Public Health, University of Alberta, Edmonton, Canada
[4] Department of Computational and Data Sciences, Indian Institute of Science, Bengaluru, India

PRC, 0000-0002-6048-0718; HW, 0000-0002-4132-6109

Pigmentation abnormalities, ranging from hypo- to hyperpigmentation, can serve as biomarkers of developmental disruption in fish exposed to environmental contaminants. However, the mechanistic pathways underlying these alterations remain poorly understood. Studies have shown that pattern formation in fish development requires specific pigment cell interactions. Motivated by experimental observations of pigmentation alterations following contaminant exposure, we investigate how pollutants influence pigment cell self-organization using a continuum reaction–diffusion–advection framework. The model incorporates non-local Morse-type kernels to describe short- and long-range interactions among melanophores and xanthophores. Our results show that perturbations to the strengths of adhesion or repulsion can drive transitions between stripes, spots and mixed patterns, reproducing phenotypes characteristic of fish pigmentation mutants. In particular, homotypic interactions are sensitive to contamination, leading to pronounced changes in melanophore density and resulting pigmentation patterns. Time-dependent simulations indicate that pigment changes from early short-term contaminant exposure may be recoverable, whereas prolonged exposure can lead to sustained pigment loss. In a growing fish, contaminant-induced changes in cell–cell interactions directly influence stripe formation rate, stripe number and pigmentation levels. Overall, our study provides insight into the mechanistic link between experimentally observed pigmentation alterations and the changes in spatial patterns of adult fish.

1. Introduction

Fish colour patterns not only provide protection from predators but also serve as important recognition signals in social communication [1]. These patterns arise from the spatial organization and interactions of pigment cells, and their formation has been extensively studied in fish [2–4]. For example, the characteristic black-and-yellow striped patterns emerge from coordinated interactions among three major pigment cell types: melanophores, xanthophores and iridophores [4–7]. These pigment cells can give rise to an incredible diversity of pigment patterns (figure 1).

Pigmentation abnormalities in fish can be triggered by a wide range of environmental pollutants. As anthropogenic activities intensify worldwide, water pollution has become a major global concern [8], with aquatic ecosystems increasingly acting as sinks for diverse contaminants [9]. Major sources of water pollution include agricultural runoff, industrial discharges and sewage effluents [10,11], which introduce a variety of pollutants such as heavy metals (e.g. mercury, lead, cadmium), excess nutrients (e.g. nitrates, phosphates),

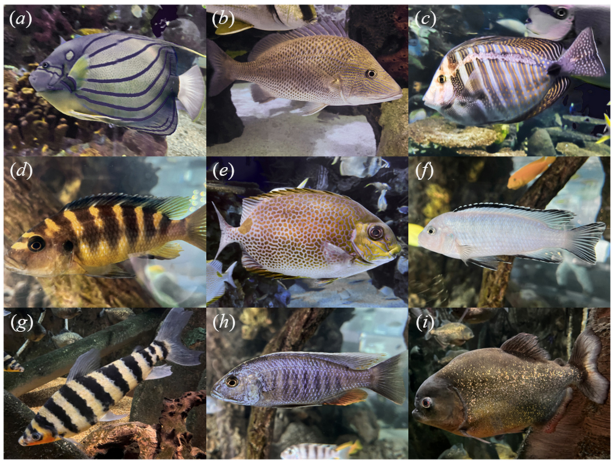

Figure 1. Examples of marine and freshwater species displaying a wide variety of pigment patterning outcomes. These patterns are determined by the number, spatial arrangement, and interactions of melanophores, xanthophores, iridophores, and other chromatophore classes. (*a*) Black-ring angelfish *Pomacanthus annularis*; (*b*) emperor bream (genus *Lethrinus*); (*c*) Desjardini sailfin tang *Zebrasoma desjardinii*; (*d*) bumblebee cichlid *Pseudotropheus crabro*; (*e*) rabbitfish (genus *Siganus*); (*f*) pale African cichlid; (*g*) banded leporinus *Leporinus fasciatus*; (*h*) electric black hap *Sciaenochromis fryeri*; (*i*) red-bellied piranha *Pygocentrus nattereri*.

industrial organic compounds (e.g. pesticides and polycyclic aromatic hydrocarbons), pharmaceuticals and microplastics. Exposure to these pollutants can alter fish pigmentation, resulting in either hypopigmentation or hyperpigmentation [12]. Hypopigmentation is typically associated with delayed development, impaired growth or pigment cell dysfunction, leading to reduced melanin production and lighter body coloration, whereas hyperpigmentation is associated with accelerated development or enhanced pigment cell activity, resulting in darker pigmentation. Several compounds have been reported to stimulate pigmentation. For example, fisetin, a natural flavonoid found in fruits and vegetables such as grapes and onions, increases both intracellular and extracellular melanin levels in B16F10 cells and enhances melanogenesis in zebrafish (*Danio rerio*) larvae [13]. Similarly, flumequine, a second-generation quinolone antibiotic known to induce phototoxicity, and rice bran ash mineral extract have been shown to stimulate pigmentation in zebrafish by upregulating key transcriptional pathways involved in melanin biosynthesis and transport [14,15]. By contrast, several contaminants have also been identified that induce hypopigmentation in zebrafish, including carbendazim and cadmium [16,17], halogenated dipeptides [18], and complex wastewater mixtures containing plasticizers, propellant precursors and aromatic compounds [19].

Proper fish pattern development requires the coordinated specification and differentiation of pigment cells, along with precise cellular interactions [20]. The absence of any one pigment-cell type disrupts the formation of normal stripe patterns. Over the past few decades, numerous experimental and theoretical studies have sought to uncover the mechanisms of pigment-cell interactions responsible for body pattern formation in fish [3,4,6,21–25]. These cellular interactions are believed to involve the ability of pigment cells to recognize one another and aggregate [26]. Using *in vitro* analyses, Yamanaka & Kondo [27] showed that adult pigment patterns are driven by direct, contact-dependent interactions between pigment cells. Such interactions can occur over short or long ranges, either through direct cell–cell contact or via protrusive structures such as pseudopodia. Ablation experiments have further confirmed that pigmentation patterns can regenerate, supporting the concept of an autonomous mechanism governed by 'short-range activation and long-range inhibition' [4].

Pollutant-induced changes in fish pigmentation are thought to occur primarily through disruptions of pigment cell–cell interactions. Many environmental contaminants can interfere with normal cellular processes by interfering with these interactions. For example, microplastics can adhere to cell surfaces through adsorption and aggregation [28] and may compromise cell walls via surface absorption [29], thereby affecting pigment formation and cell–cell communication. Similarly, widely distributed chemicals such as bisphenol A (BPA) and bisphenol F can alter melanin synthesis in zebrafish embryos [19], with BPA disrupting integrin signalling and lipid raft domains that are critical for proper cell adhesion and signalling [30]. Heavy metals, such as lead (Pb), can further compromise cellular integrity by altering the molecular composition of proteins, lipids and DNA, leading to protein degeneration and lipid peroxidation [31]. Moreover, some endocrine-disrupting chemicals can modify gene expression in immune cells, affecting cell–cell interactions and overall cellular communication networks [32]. Overall, data suggest that a diversity of pollutants may alter pigment via cell interactions, ultimately disrupting the normal pattern formation in fish.

Theoretical modelling provides a powerful framework for qualitatively and quantitatively exploring pigment cell interactions. Since Alan Turing proposed a hypothetical mechanism in 1952 to explain patterns observed in animal skin [33], numerous theoretical studies have focused on cell interactions using continuum partial differential equation models, lattice-based cellular automata and agent-based modelling approaches [3,23,34]. However, to date, no studies have specifically examined the effects of environmental contaminants on pigment cell interactions. Understanding how water contaminants influence developmental processes in aquatic organisms requires a mechanistic framework that links observed biological patterns with underlying cellular and physical mechanisms. To address this gap, we incorporate pollutants into a model of pigment cell interactions to examine how contaminants affect cell–cell communication, proliferation, migration and short- or long-range signalling. In particular, we

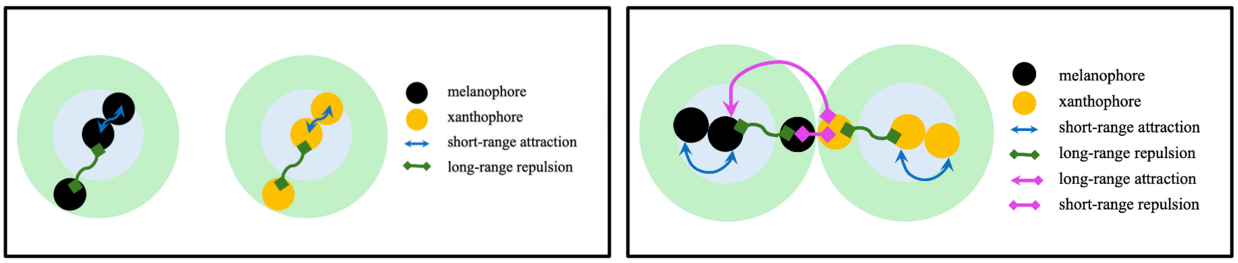

(a) Homotypic (b) Heterotypic

Figure 2. Illustrations of homotypic and heterotypic interactions. (a) In the homotypic case, only short-range attraction and long-range repulsion occur among cells of the same type, with no interactions between different cell types. (b) In the heterotypic case, an additional one-directional long-range attraction and a short-range repulsive interaction between the two cell types are present, producing a chase-and-run type of behaviour in which xanthophores chase melanophores while melanophores avoid xanthophores.

formulate a general reaction–diffusion–advection model to investigate hypo- and hyperpigmentation under varying levels of water pollutants.

Most chemical pollutants in aquatic environments rarely reach lethal levels, highlighting the importance of studying sub-lethal effects to capture the full spectrum of adverse chemical impacts on aquatic species. Sub-lethal exposures are expected to induce subtle changes, such as in cell interactions, rather than cause cell death. From a mathematical perspective, our approach allows us to identify which pigment cell interactions are most sensitive to pollutant exposure and most likely to be disrupted, potentially giving rise to mutant pigmentation patterns [35]. We also conducted complementary experiments involving methane exposure to further support these findings.

2. Pattern formation driven by melanophore–xanthophore interactions

Pigment cells can interact over both short and long ranges [27]. Short-range interactions involve direct cell–cell contact or communication mediated by short dendritic extensions. By contrast, long-range interactions are facilitated by melanophores extending elongated protrusions, known as pseudopodia, which transmit signals to cells located at a longer distance [36]. Contact-dependent cell adhesion promotes cell–cell attachment and aggregation, whereas cell–cell repulsion prevents overcrowding and maintains appropriate intercellular spacing, thereby sharpening the boundaries of pigment patterns. Although several pigment cell types contribute to fish coloration, interactions between melanophores and xanthophores alone are sufficient to generate self-organized body patterns [6]; these two cell types are the focus of this study. Genetic analyses have revealed the presence of homotypic interactions among melanophores and xanthophores [26]. Homotypic interactions, occurring between cells of the same type (melanophore–melanophore and xanthophore–xanthophore), play a crucial role in pigment cell proliferation, dispersal, and tiling within the skin [1]. By regulating intercellular spacing, these interactions ensure a well-distributed layer of each pigment cell type across the fish's body.

Heterotypic interactions occur between melanophores and xanthophores. Xanthophores extend pseudopodia towards melanophores, inducing melanophore movement away from the contact site, while xanthophores actively pursue them (figure 2), giving rise to a 'run-and-chase' behaviour. In the literature, heterotypic interactions are primarily shown to determine the stripe pattern formation, while homotypic interactions regulate the number of cells, direction of migration and individual spacing of cells within chromatophore populations [1]. Together, these coordinated interactions generate the distinct spatial organization of pigment cells that underlies fish colour pattern formation.

2.1. Modelling pigment cell interactions for pattern formation

Let $u(x,t)$ and $v(x,t)$ denote the densities of melanophores and xanthophores, respectively. We approximate the fish surface as a two-dimensional spatial domain $\Omega \subset \mathbb{R}^2$. These cells interact through migration, proliferation and death. Migration is modelled as a combination of random diffusion and directed, non-local advection driven by cell–cell interactions, while proliferation and death are described by local interaction terms $f(u,v)$ and $g(u,v)$. The resulting reaction–diffusion–advection system is

$$\begin{aligned} u_t &= D_u \Delta u - D_{uv} \nabla \cdot \big(u \nabla (G_{uv} * v)\big) - D_{uu} \nabla \cdot \big(u \nabla (G_{uu} * u)\big) + f(u,v), \quad \text{in } \Omega \times (0,T), \\ v_t &= D_v \Delta v - D_{vu} \nabla \cdot \big(v \nabla (G_{vu} * u)\big) - D_{vv} \nabla \cdot \big(v \nabla (G_{vv} * v)\big) + g(u,v), \quad \text{in } \Omega \times (0,T). \end{aligned} \tag{2.1}$$

Here, D_u and D_v denote the diffusion coefficients of melanophores and xanthophores, respectively. The directed movement is governed by interaction kernels G_{ij}, chosen as truncated Morse potentials to capture both attractive and repulsive forces within a

finite interaction range [37]:

$$G_{ij}(x,y) = \begin{cases} A_{ij}\mathrm{e}^{-(x^2+y^2)/d_{ij}^a} - R_{ij}\mathrm{e}^{-(x^2+y^2)/d_{ij}^\rho}, & (x^2+y^2) \le d_a, \\ 0, & \text{otherwise}, \end{cases}$$

where $i,j \in \{u,v\}$. Each kernel has compact support within a disk of radius d_a, reflecting the maximum distance over which cells interact directly or via protrusions such as pseudopodia. The parameters A_{ij} and R_{ij} denote the strengths of attraction and repulsion, while d_{ij}^a and d_{ij}^ρ represent the corresponding interaction length scales.

The convolution operator

$$(G_{ij} * j)(x,y) = \int_\Omega G_{ij}(x-x',\, y-y')\, j(x',y')\, \mathrm{d}x'\, \mathrm{d}y'$$

describes the cumulative non-local influence of cells of type j on cells of type i at position (x,y). The homotypic kernels G_{uu} and G_{vv} describe interactions between cells of the same type, whereas the heterotypic kernels G_{uv} and G_{vu} describe interactions between different cell types: G_{uv} captures the influence of xanthophores on melanophores, and G_{vu} captures the effect of melanophores on xanthophores. The coefficients D_{uu}, D_{uv}, D_{vu} and D_{vv} quantify the strength of these interaction-induced advective effects. The advective terms $\nabla \cdot (u\nabla(G_{uv} * v))$ and $\nabla \cdot (u\nabla(G_{uu} * u))$ represent directed movement of melanophores in response to heterotypic and homotypic interactions, respectively. Depending on the balance between attractive and repulsive components of the interaction potentials, these forces can drive cells either towards or away from one another. The interplay of diffusion, non-local interactions and local growth dynamics ultimately gives rise to self-organized pigment patterns on the fish body.

The well-posedness of the model has been extensively studied in the literature, including cases with less regular interaction kernels [38,39]. For numerical simulations, we consider a static two-dimensional domain representing a portion of the fish surface, with periodic boundary conditions. Due to the complexity of system equation (2.1), it is generally not possible to determine the full parameter space from experimental data. Therefore, rather than exploring all possible emergent patterns, we focus specifically on spot and stripe formations. The diffusion parameters are chosen based on ranges previously used to simulate spot patterns in fish leopard mutants [40]. The interaction strengths are set uniformly as $D_{uu} = D_{uv} = D_{vu} = D_{vv} = 0.01$, while the random motility coefficients are $D_u = D_v = 0.1$. To generate spot patterns, the system is initialized with small random perturbations around mean cell densities:

$$u_0 = u_{00} + \varepsilon_1\xi_1(x,y), \quad v_0 = v_{00} + \varepsilon_2\xi_2(x,y), \tag{2.2}$$

where ξ_1 and ξ_2 are random fields.

Local reaction kinetics. The cell proliferation and death of melanophores and xanthophores are governed by the local reaction terms, denoted by $f(u,v)$ and $g(u,v)$, respectively. In our modelling assumptions, we consider density-dependent cell proliferation, where growth is proportional to the cell density at low concentrations and decreases as local crowding increases. This is represented by the logistic terms $u(1-u)$ and $v(1-v)$ for the proliferation of u and v, respectively. Furthermore, experimental and theoretical studies suggest that, at short distances, there is competition between xanthophores and melanophores, which leads to competition for space and induces crowding-related death [3,4]. Therefore, we model the reaction terms as

$$f(u,v) = u(1-u-v), \quad g(u,v) = v(1-v-u).$$

This minimal formulation of the reaction terms allows us to isolate and investigate the effects of homotypic and heterotypic interactions through the non-local kernels G_{ij} in pattern formation. In this sense, our model provides a minimal yet mechanistically interpretable description of pigment pattern formation.

Homotypic and heterotypic cell interactions. Pattern formation arises due to attractive and repulsive forces between interacting cells. Exposure to toxic pollutants can disrupt these interaction mechanisms by altering cell kinetics, adhesion strength and cell communication. In our system, we assume that the fish is continuously exposed to an external pollutant and this exposure can influence the interaction strength between melanophores and xanthophores. In our study, homotypic and heterotypic cellular interactions are described through the spatial kernel G_{ij}, where $i,j \in \{u,v\}$. These interactions capture density-dependent movement driven by the spatial distribution of cells of the same type (homotypic) or of different types (heterotypic), without directly influencing the local growth and death processes. We consider homotypic interactions by setting $G_{uv} = G_{vu} = 0$ in the model equation (2.1). This incorporates short-range attraction and long-range repulsion among cells of the same type, such that $d_{uu}^a < d_{uu}^\rho$ and $d_{vv}^a < d_{vv}^\rho$ (figure 2a). In this case, the model equation (2.1) accounts only for interactions between u–u and v–v cells in the non-local advection terms:

$$G_{uu} = \begin{cases} A_{uu}\mathrm{e}^{-r^2/d_{uu}^a} - R_{uu}\mathrm{e}^{-r^2/d_{uu}^\rho}, & r^2 \le d_u^e \\ 0, \quad \text{otherwise} \end{cases} \qquad G_{vv} = \begin{cases} A_{vv}\mathrm{e}^{-r^2/d_{vv}^a} - R_{vv}\mathrm{e}^{-r^2/d_{vv}^\rho}, & r^2 \le d_v^e \\ 0, \quad \text{otherwise}, \end{cases} \tag{2.3}$$

where $r^2 = x^2 + y^2$. The long-range repulsion parameters are set as $d_{uu}^\rho = 3d_{uu}^a$ and $d_{vv}^\rho = 3d_{vv}^a$, while effective cut-off distances are $d_u^e = 5d_{uu}^a$ and $d_v^e = 5d_{vv}^a$ beyond which cells do not interact. In contrast to the homotypic case, heterotypic interactions capture

how u and v cells influence each other's movement through cross-interaction kernel terms. *In vitro* experiments describe these interactions as directed movement, where melanophores move away from xanthophores, while xanthophores actively pursue melanophores, giving rise to the characteristic 'run-and-chase' behaviour [6,41,42]. We capture this asymmetry using short-range repulsion in both directions and one-directional long-range attraction as follows:

$$G_{uv} = \begin{cases} A_{uv}e^{-r^2/d_{uv}^a} - R_{uv}e^{-r^2/d_{uv}^\rho}, & r^2 \le d_{uv}^e \\ 0, \quad \text{otherwise} \end{cases} \qquad G_{vu} = \begin{cases} -R_{vu}e^{-r^2/d_{vu}^\rho}, & r^2 \le d_{vu}^e \\ 0, \quad \text{otherwise}, \end{cases} \tag{2.4}$$

where $R_{uv} > A_{uv}$. The short-range repulsion distances are taken equal such that $d_{uv}^\rho = d_{vu}^\rho$, and the long-range attraction for G_{uv} is set to $d_{uv}^a = 3d_{uv}^\rho$. The effective cut-off distance is $d_{uv}^e = d_{vu}^e = 5d_{uv}^\rho$, beyond which the cells do not interact. The heterotypic interaction, therefore, captures both the intercellular and intracellular interactions (figure 2b). Under these settings, the model produces Turing-like spot patterns, comparable to those observed in leopard mutant fish [43], with variations in spot size, density and connectivity corresponding to different alleles [21]. Thus, our reaction–diffusion–advection model equation (2.1) effectively captures the formation of pigment patterns in fish. In the upcoming sections, we investigate how external pollutants perturb the homotypic and heterotypic cellular interactions over short and long spatial scales, thereby influencing the pigment pattern formation.

3. Pollutants lead to pigmentation changes

As pigment patterns in various fish mutants largely result from specific pigment cell–cell interactions, alterations or loss of pigmentation indicate that exposure to environmental pollutants may disrupt these fundamental cellular mechanisms. Motivated by this, we investigate the effects of pollutants on each pigment cell type individually, aiming to identify which interactions are most sensitive to chemical exposure.

Pollutant-induced hyper- and hypopigmentation. Exposure to certain environmental contaminants can alter fish pigmentation, leading to either hypopigmentation or hyperpigmentation. Some compounds have been reported to stimulate pigmentation and produce darker patterns. For instance, fisetin [13], flumequine [14] and rice bran ash mineral extract [15] enhance melanogenesis by promoting melanin biosynthesis and transport. Conversely, several contaminants are associated with hypopigmentation. Carbendazim and cadmium, for example, reduce pigment deposition [16,17]. Exposure to *N*-(1,3-dimethylbutyl)-*N*′-phenyl-*p*-phenylenediamine (6PPD) significantly decreases melanin in larval zebrafish [44]. Similarly, the disinfection by-product 3,5-di-L-iodotyrosylalanine (DIYA), although not acutely toxic to embryonic zebrafish, significantly inhibits pigmentation in melanophores and xanthophores of the head, trunk and tail at higher concentrations [18].

Our experimental results: methane-induced hypopigmentation. In our experiment, zebrafish larvae were exposed to methane (CH_4) for four consecutive days at concentrations of 10%, 20% and 25% (by gas volume; oxygen concentration was not altered). After 4 days post-fertilization (dpf), larvae were returned to normal water, while a parallel control group was maintained under identical conditions without methane. Each group consisted of six to eight larvae. Our results (figure 3) show progressive hypopigmentation with increasing methane exposure. The pale coloration reflects delayed melanin development, with quantitative analysis indicating an approximately 10% reduction in melanin in larvae exposed to 25% methane. This inhibitory effect is spatially heterogeneous, with the tail showing the most pronounced reduction, nearly 20% greater than the head (figures 3 and 4). Representative images and summarized data are provided in figure 4 and table S1 in the supplementary material.

Pollutants can influence cell–cell interactions. Fish pigmentation patterns (e.g. stripes, spots, and patches) are determined by the number, type and spatial arrangement of pigment cells, including melanophores, xanthophores and iridophores [20]. A growing body of evidence shows that environmental pollutants can affect organisms by disrupting fundamental cell–cell interactions [45]. Pollutants are often present at low concentrations and as complex mixtures, and they can produce synergistic, antagonistic or additive effects that interfere with normal developmental processes. Pollutants can damage cells through multiple pathways, including oxidative stress, mitochondrial dysfunction, inflammation and proteotoxicity [46]. For instance, widely distributed chemicals such as microplastics can adhere to cell membranes, blocking signal transport and impairing protein synthesis [29]. Other contaminants, including resin acids, cadmium, lead and monochloramine, can disrupt chemical signalling and induce abnormal cell morphologies [47], while BPA interferes with integrin signalling and lipid raft domains essential for proper cell adhesion and communication [30]. Of specific relevance here, a wide array of organic contaminants can interfere with the cell membrane at its surface, or through partitioning into the three-dimensional interior of the lipid bilayer [48]. These interactions, referred to as polar and non-polar narcosis, can alter the function of membrane-bound proteins, which may be key to cell–cell interactions. Regardless of route, pigment cell systems are highly sensitive to chemical disturbances. Experiments in zebrafish demonstrate that when pigment cells in a localized region are ablated, new cells regenerate the pattern; however, their development and survival strongly depend on interactions with surrounding cells [4]. Adjacent melanophores and xanthophores exhibit mutual repulsion, maintaining the boundaries of pigment patterns [40]. These findings collectively suggest that pollutants can perturb a wide range of cellular interaction mechanisms, providing a strong biological rationale for studying how altered intercellular communication may lead to abnormal pigment patterns in developing fish.

Our experimental results: methane alters pigment cell–cell interactions. Quantitative image analysis revealed a pronounced loss of continuous stripe patterns and increased fragmentation of pigment patterns in 4 dpf zebrafish larvae exposed to 25% CH_4. Within the region of interest, control larvae exhibited fewer pigment regions primarily due to the formation of a continuous stripe in the

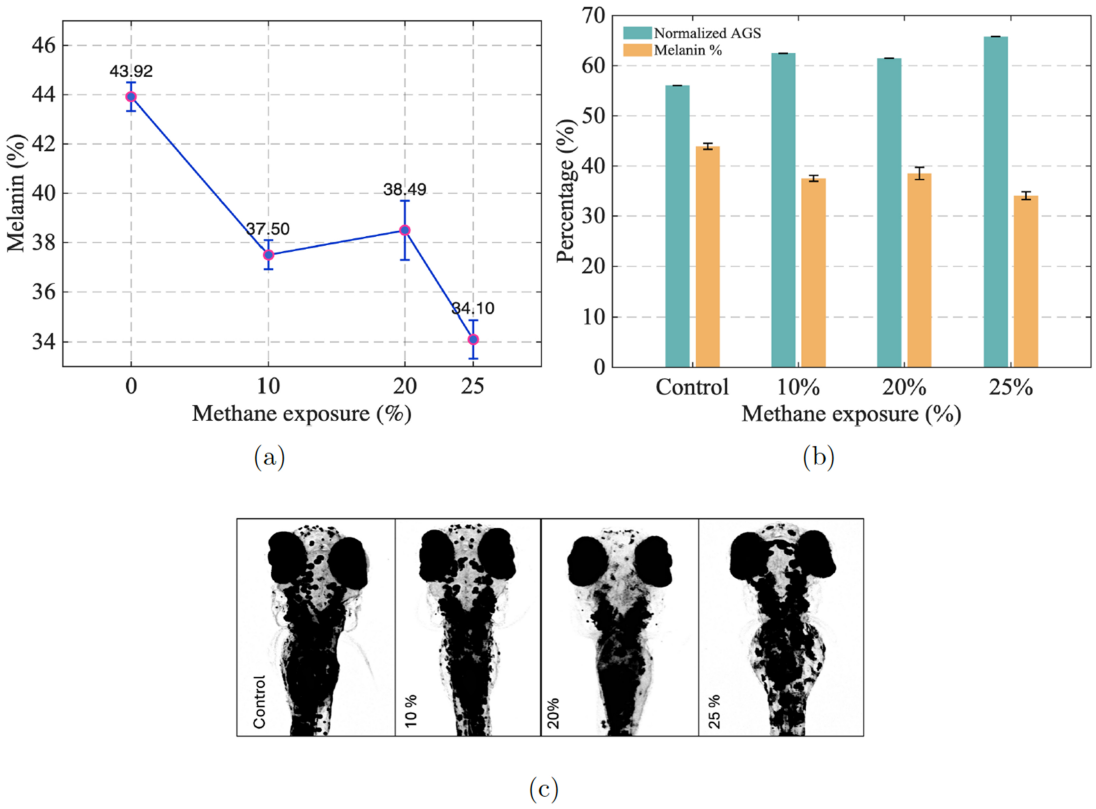

Figure 3. Inhibition of melanin pigmentation in zebrafish larvae at 4 dpf exposed to methane at different concentrations (6–24 fish samples considered for each concentration). (a) Melanin percentage in the head–dorsal region at different exposure levels; (b) histogram of average greyscale (AGS) and melanin percentage for control and methane-exposed larvae; (c) dorsal view of the head region of a zebrafish sample used in the experiment.

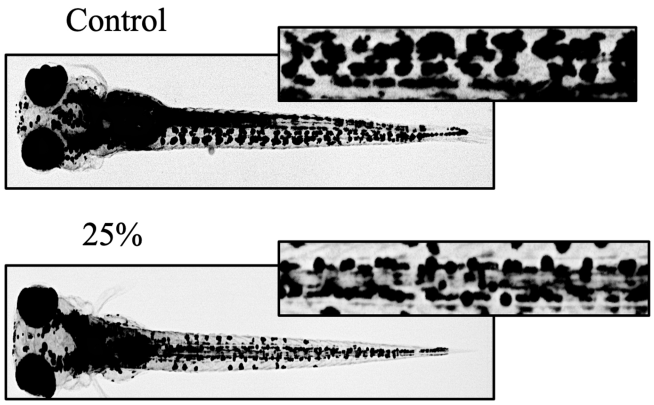

Figure 4. Localized inhibition of pigmentation near the tail region in zebrafish larvae exposed to 25% CH_4 at 4 dpf compared to control.

mid-body region (count = 8), a larger average region size (1080) and greater overall pigment coverage (area = 29.1%) (left panel of figure 5).

This large average region size reflects the presence of the developing stripe, which is a natural stage of zebrafish pattern formation. By contrast, methane-exposed larvae failed to form this stripe and instead exhibited a substantially higher number of fragmented pigment regions (count = 20), accompanied by a marked reduction in average region size (272) and total pigment coverage (area = 18.3%) (right panel of figure 5).

Together, these metrics indicate enhanced fragmentation, with pigment cells forming smaller and more spatially disconnected clusters under methane exposure. While control larvae at 4 dpf begin to develop a coherent stripe in the central body region, methane exposure disrupts this process, reducing stripe continuity and impairing early pattern formation. This fragmentation suggests a disruption of normal melanophore aggregation dynamics, which are essential for stripe development. These experimental observations motivate the hypothesis that pollutant exposure alters cell–cell signalling, mathematically represented through the kernel functions, thereby regulating pigment pattern formation.

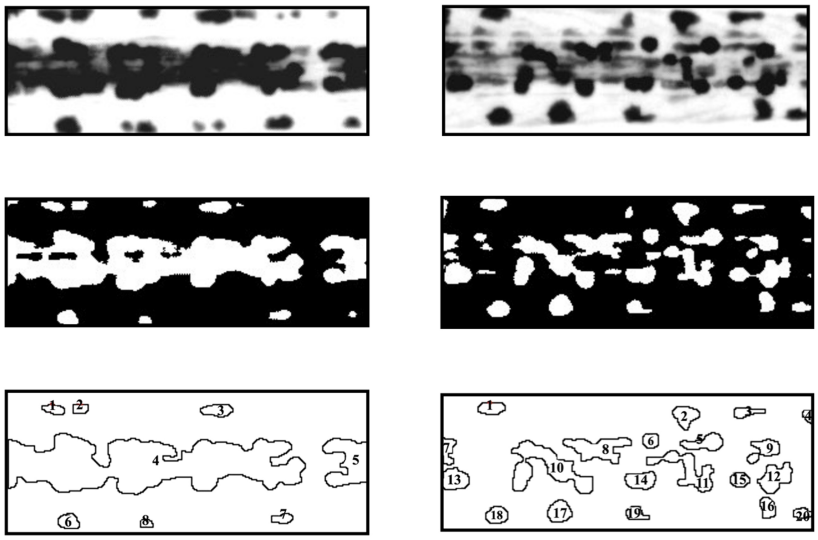

Figure 5. Image analysis of pigmentation patterns at 4 dpf. The left panel shows normal continuous stripe development in a control larva, along with the thresholded image and identified connected pigment regions. The right panel shows disrupted stripe formation and enhanced fragmentation in a larva exposed to 25% CH_4, with thresholded images revealing a larger number of spatially disconnected pigment regions. The analysis was performed using ImageJ [49], and the bottom panel shows the number of fragmented regions.

Pigment cell–cell interactions drive pattern changes. Perturbations induced by pollutants or other environmental factors that disrupt this balance will eventually alter adult patterns. For instance, the zebrafish mutant *touchtone*^{b722} (*tct*) lacks neural crest-derived melanophores and the remaining differentiated melanophores are pale and reduced in size [50]. The *nacre* mutant lacks all neural crest-derived melanophores, while *pfeffer* exhibits severely reduced numbers of xanthophores, resulting in the breakdown of stripes into spots. The simultaneous absence of melanophores and xanthophores produces the double mutant *nac;pfe*. By contrast, mutants such as *leopard* and *seurat* display spot-like patterns instead of stripes, whereas *obelix* exhibits broadened stripes [43].

Early pigment alterations impact later development. Many studies examining the effects of pollutants on fish pigmentation focus on larvae, yet early pigment alterations can have long-lasting consequences. Pigment cells specified and patterned during embryonic and early larval stages subsequently undergo differentiation and metamorphosis to form adult pigment patterns [51]. In zebrafish, neural crest-derived melanophores differentiate during embryogenesis to generate early larval pigment stripes [52]. This pattern features xanthophores dispersed over the flank, while melanophores and iridophores are positioned along the dorsal and ventral edges, over the yolk, and along a lateral stripe following the horizontal myoseptum [53]. During metamorphosis, these embryonic melanophores are gradually replaced by newly differentiating metamorphic melanophores, ultimately forming adult stripes [52]. The early larval pattern is thus remodelled into the adult configuration, consisting of alternating dark stripes of melanophores and iridophores and light stripes of xanthophores and iridophores [53]. Disruptions during embryogenesis can significantly impact adult pattern formation [54], as proper stripe development depends on coordinated pigment cell lineage specification, differentiation, specific cellular interactions and morphogenetic behaviours [20]. On the other hand, even when early larval pigmentation appears normal, disruptions to embryonic signalling pathways may lead to defects in adult patterning. Mutants that display normal embryonic pigmentation but defective adult patterns reveal critical factors for establishing, maintaining or recruiting metamorphic melanophore precursors. For example, the zebrafish mutant *picasso* lacks most metamorphic melanophores due to mutations in the ErbB gene *erbb3b*, which encodes an epidermal growth factor receptor-like receptor tyrosine kinase. This highlights a critical embryonic critical period for ErbB signalling in promoting later pigment pattern metamorphosis, despite normal early melanophore patterns [52].

Explanation for pollutant-induced pattern changes. From a developmental perspective, environmental pollutants may either generate genetic mutations or act as exogenous perturbations that interfere with the cellular processes responsible for normal pigment pattern formation [16,17,43,44,55]. A plausible mechanism underlying pollutant-induced pigmentation changes is that contaminants entering the organism disrupt developmental signalling pathways, oxidative balance or cellular metabolism [56,57]. Such disruptions can impair pigment cell specification, migration, survival or differentiation, thereby altering pigment cell–cell interactions during critical developmental windows. Adult stripe and spot patterns emerge from a finely balanced interplay of adhesive and repulsive interactions among melanophores, xanthophores and iridophores [4,20]. Pollutant-induced perturbations to this balance can therefore translate into observable changes in pigmentation patterns. Even modest changes in signalling strength, motility or survival of a single pigment cell type may propagate through intercellular interactions, ultimately leading to large-scale reorganization of the final pigment pattern. This perspective provides a mechanistic link between environmental contamination, developmental toxicity and the emergence of abnormal pigmentation patterns in adult fish.

4. Results

To investigate the effects of pollutants on fish pigmentation patterns, we incorporate their influence into the model. Assuming pollutants are approximately uniform locally, we model the pollutant level as a constant background level T_0 with small random fluctuations:

$$T(x, y) = T_0 + \varepsilon\eta(x, y),$$

where $\eta(x, y)$ is a randomly chosen function taking values in $[0, 1]$, and ε is a small perturbation parameter.

Different pollutants can have diverse effects on pigmentation, including reduced pigmentation, hyperpigmentation or irregular patterns [58,59]. Since fish stripe and spot patterns emerge from a finely balanced interplay of adhesive and repulsive interactions among melanophores, xanthophores and iridophores [4], these observations suggest that pollutants can perturb this balance in multiple ways. Within a reaction–advection–diffusion framework, such exposure can be represented as changes in interaction kernel strengths. We therefore examine representative cases of homotypic and heterotypic interactions under pollutant exposure to understand how alterations in pigment cell interactions lead to diverse pigmentation patterns. While experimental studies provide valuable observations, mathematical modelling enables a systematic exploration of how specific changes in cell–cell interactions propagate to influence overall pattern formation. This approach also allows us to investigate the effects of varying pollutant levels, timing, or modes of action, identify interactions most sensitive to disruption, and test hypothetical scenarios that are difficult to study experimentally.

4.1. Pollutant-induced changes in homotypic and heterotypic cell interactions

Chromatophore patterning in a species is determined by a fine balance between adhesive and repulsive forces among cells. Thus, any biologically meaningful hypothesis must involve a structured perturbation of this balance. The following hypotheses explore how specific disruptions in cell–cell interactions, induced by increasing contaminant concentration, could reproduce distinct spatial patterns that resemble mutant-like phenotypes. From a mechanistic standpoint, contaminants can disrupt pigmentation by altering both homotypic and heterotypic interactions between melanophores and xanthophores. Accordingly, we formulate a set of hypotheses to represent these potential interaction-level perturbations. Together, these interactions establish the spatial arrangement of pigment cells that underlie characteristic colour patterns in fish. Environmental pollutants can interfere with cell–cell interaction pathways in different ways, potentially affecting these two interaction mechanisms differently. In our framework, these interactions are represented through non-local kernels rather than reaction kinetics. Therefore, we specifically model pollutant-induced perturbations to the kernel functions through the following hypotheses.

(HM1) The pollutant reduces repulsion between cells while enhancing short-range adhesion until reaching a saturating threshold. We model this as $R_{uu}(T(x,y)) = R_{uu}\left(\frac{1}{1+T(x,y)}\right)$, $R_{vv}(T(x,y)) = R_{vv}\left(\frac{1}{1+T(x,y)}\right)$, and $A_{uu}(T(x,y)) = A_{uu}\left(1+\frac{T(x,y)}{1+T(x,y)}\right)$, $A_{vv}(T(x,y)) = A_{vv}\left(1+\frac{T(x,y)}{1+T(x,y)}\right)$, where $T(x,y)$ is the pollutant field over the domain. The saturating functional form is motivated by the dose–response curve of hypopigmentation with exposure concentration (see the supplementary material). The mathematical description of each of the hypotheses is described in the supplementary material. Here, the net attractive potential among $u-u$ cells is greater than that of $v-v$ cells. As shown in figure 6b, spot patterns partially break down, producing a mixture of spots and stripes.

(HM2) The pollutant increases melanophore attraction while decreasing their repulsion, with the opposite effect for xanthophores (increased repulsion and reduced attraction). This combination ensures strong mutual attraction among melanophores and strong repulsion among xanthophores. Despite enhanced melanophore attraction, black spot patterns disappear, indicating that xanthophore repulsion is critical for maintaining black pigmentation (cf. figure 6c).

(HM3) The pollutant increases net repulsion for both xanthophores and melanophores while reducing attraction. Although a spot pattern similar to that of the control persists, the maximum melanophore density (u) is significantly lower, and the overall coloration is lighter, indicating hypopigmentation (cf. figure 6d).

(HM4) Without influencing xanthophore interactions, the pollutant only increases repulsion and decreases attraction among melanophores as contaminant concentration rises. In this case, melanophores experience a net repulsive potential, causing the spot pattern from the control to break down into irregular stripe patterns (upper panels of figure 6).

As can be seen in figure 6, different pollutant-induced changes in cell interactions can generate diverse mutant-like body patterns. From maximum melanophore densities, cases HM2 and HM3 produce hypopigmentation, while a purely repulsive potential among xanthophores can induce hypopigmentation without disrupting the overall pattern structure. These results demonstrate how pollutants modulate cell–cell interactions to drive variations in fish pigmentation.

We next investigate the effects of pollutants on heterotypic interactions. Specifically, we consider several representative scenarios in which pollutant exposure alters the attractive and repulsive forces governing heterotypic interaction potentials. The resulting interaction kernels and corresponding pattern outcomes are shown in figure 7, where distinct potential profiles emerge under different pollutant-induced perturbations.

(HT1) Pollutant exposure enhances the short-range repulsion exerted by melanophores on xanthophores.

(HT2) The pollutant simultaneously increases the repulsion exerted by melanophores on xanthophores while weakening their long-range attraction, rendering the attractive and repulsive contributions comparable in magnitude.

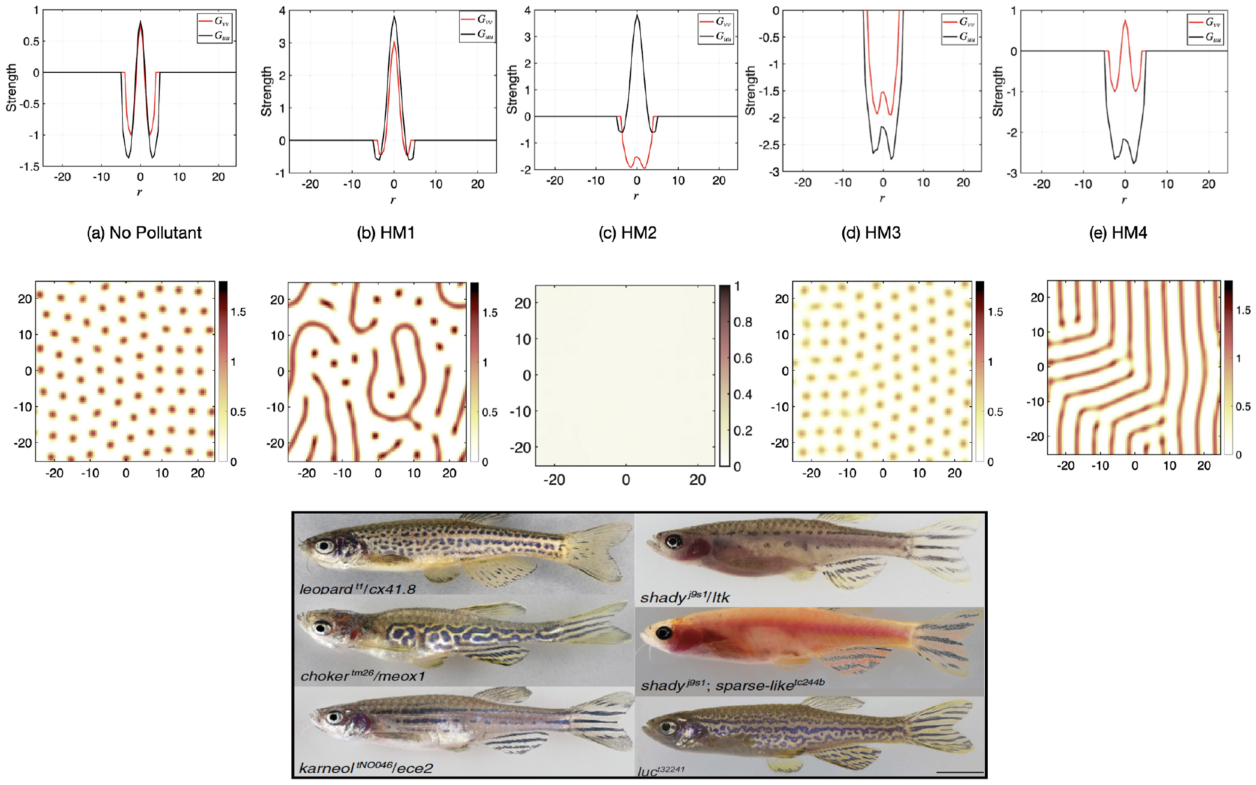

Figure 6. The kernel functions and pigment pattern formation in two-dimensional spatial domain Ω considering the homotypic interaction between the melanophores (black) and xanthophores (yellow) at $t = 300$. Upper panel: The change in the kernel functions due to the incorporation of pollutants. Middle panel: The simulated patterns due to the effect of corresponding kernels. Bottom panel: Some of the representative mutant images of zebrafish adapted from [43,60]. The parameters chosen for simulations are $R_{vv} = 3, A_{uu} = 5, A_{vv} = 4, d_{uu} = 5$ and $d_{vv} = 3$. We consider the pollutant field as $T(i,j) = 0.5 + 0.1\,\eta(i,j)$, and the initial conditions are taken as $u_0(i,j) = 1 + 0.01\,\xi_1(i,j)$ and $v_0(i,j) = 1 + 0.02\,\xi_2(i,j)$, where $\xi_k(i,j) \overset{\text{i.i.d.}}{\sim} \mathcal{N}(0,1)$.

(HT3) The pollutant strengthens the long-range attraction of melanophores towards xanthophores while reducing short-range repulsion.

(HT4) Pollutant exposure reduces both short-range repulsive interactions—melanophore-on-xanthophore and xanthophore-on-melanophore.

For all four heterotypic cases, although pollutant exposure induces distinct modifications to interaction strengths, the resulting patterns remain largely similar to the pollutant-free control. Among these scenarios, only HT3 leads to a noticeable change in pattern and hyperpigmentation (cf. figure 7d). The homotypic case exhibits a pronounced reduction in the maximum melanophore density under hypothesis HM2. By contrast, pollutants seem to have a weaker effect on heterotypic interactions, with the $\max(u)$ density remaining within a narrow range across all simulated hypotheses (cf. figure 8a). This indicates that homotypic interactions are considerably more sensitive to pollutant-induced perturbations. In homotypic scenarios, the maximum melanophore density varies widely, from approximately 0.1 to 1.7, with changes of up to 90%, whereas in heterotypic cases it remains within a narrower range of 1.91–2.21, with the maximum change across all cases being no more than 9% compared with the control. We further investigate pigmentation by comparing the mean melanophore density in the homotypic and heterotypic cases. The mean density is defined as the spatial average of pigment concentration over the domain Ω, given by

$$\langle u \rangle = \frac{1}{|\Omega|} \int_{\Omega} u(x,y)\,\mathrm{d}x\,\mathrm{d}y. \tag{4.1}$$

Figure 8b shows the mean melanophore density $\langle u \rangle$ at time $t = 300$. Both the homotypic and heterotypic cases exhibit reduced mean density under hypotheses HM2/HT2. The mean density of u cells in the homotypic case shows greater variability, whereas the heterotypic case exhibits a more gradual variation. Although both local and global metrics are used to investigate hypo- and hyperpigmentation, the qualitative conclusions remain consistent across these measures (compare figure 8a,b), demonstrating the robustness of our results. To quantify the spatial extent of pigmentation, we compute the fraction of the domain where the pigment intensity exceeds a threshold. Since each hypothesis represents a different mechanism, a fixed threshold would be misleading. Therefore, we adopt an adaptive threshold $\langle u \rangle^k_{\text{ad}}$, based on the mean melanophore density $\langle u \rangle$ for each homotypic and heterotypic case (k). We define

$$F = \frac{1}{|\Omega|} \int_{\Omega} \mathbf{1}_{\{u(x,y) \geq \langle u \rangle^k_{\text{ad}}\}}\,\mathrm{d}x\,\mathrm{d}y,$$

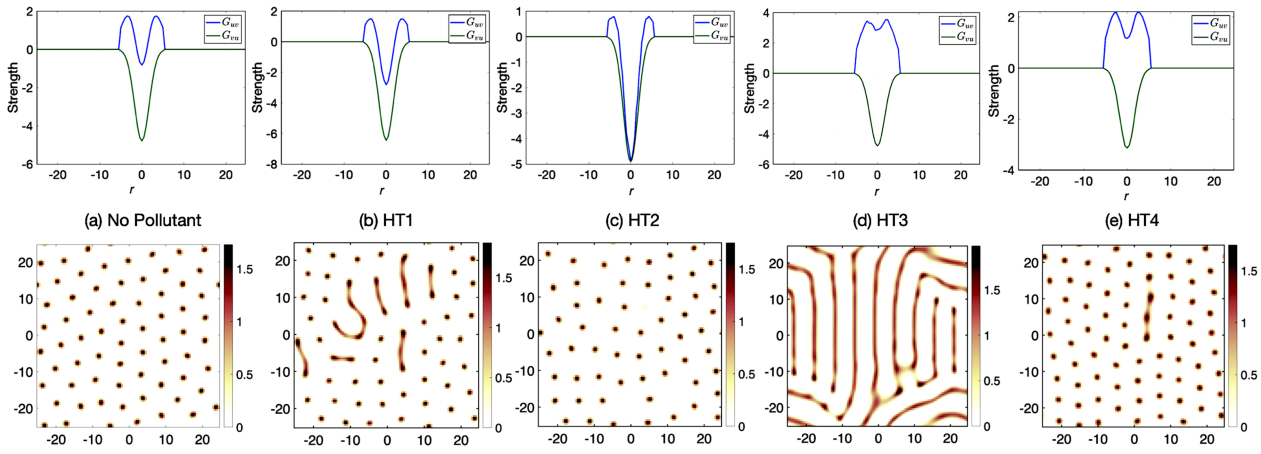

Figure 7. The kernel functions and pigment pattern formation in two-dimensional spatial domain Ω considering the heterotypic cellular interaction between the melanophores (black) and xanthophores (yellow) at $t = 300$. Upper panel: The change in the kernel functions G_{uv} and G_{vu} due to the incorporation of an external pollutant. Lower panel: The pattern formation due to the effect of the corresponding kernels. The homotypic interaction parameters R_{vv}, A_{uu}, A_{vv}, d_{uu}, and d_{vv} are kept fixed as in figure 6, and the heterotypic parameters are $R_{uv} = 6$, $A_{uv} = 5$, $R_{vu} = 5$ and $A_{vu} = 0$, and the interaction range $d_{uv} = 6$. We choose the pollutant field for the simulation $T(i,j) = 0.5 + 0.1\,\eta(i,j)$. The initial conditions: $u_0(i,j) = 1 + 0.01\,\xi_1(i,j)$ and $v_0(i,j) = 1 + 0.02\,\xi_2(i,j)$, and $\xi_k(i,j) \overset{\text{i.i.d.}}{\sim} \mathcal{N}(0,1)$, $k = i,j$.

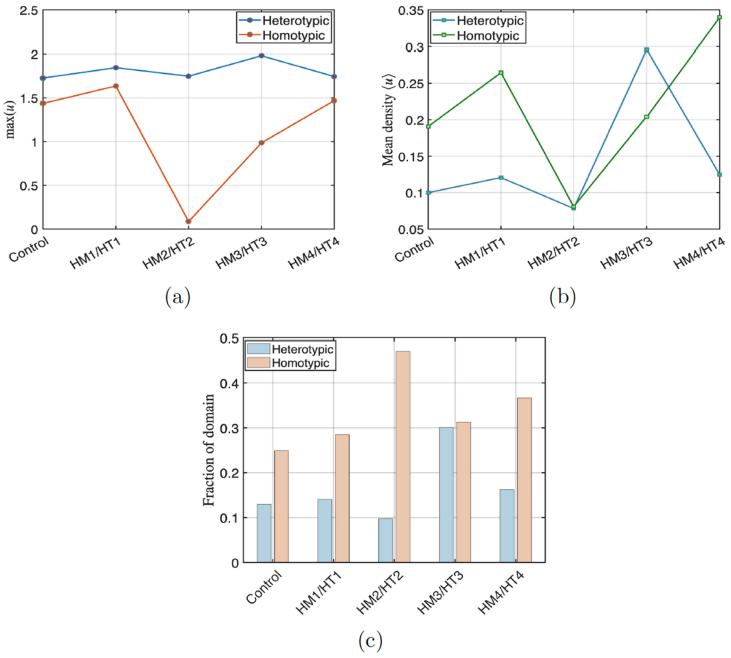

Figure 8. Comparison of (a) the maximum melanophore density $\max(u)$, (b) the mean melanophore density $< u >$ and (c) the spatial extent of the melanophores is shown by calculating the fraction of the domain greater than the mean density of melanophores for the pattern obtained for the different homotypic and heterotypic interactions in figures 6 and 7.

where $\mathbf{1}_{\{u(x,y)\geq\langle u\rangle^k_{\text{ad}}\}}$ denotes the indicator function. This quantity is approximated numerically as the proportion of grid points satisfying $u_{ij} > \langle u\rangle^k_{\text{ad}}$. Figure 8c shows a clear difference between the homotypic and heterotypic cases. Across all hypotheses, homotypic interactions consistently show higher spatial coverage than heterotypic interactions, indicating a more widespread distribution of pigment cells in the presence of pollutants. By contrast, heterotypic interactions exhibit less variability under pollutant exposure relative to the control case.

4.2. Pigmentation responses to increasing pollutant levels

The different cases of cell interaction changes were tested under varying levels of pollutant exposure, using the control (no-pollutant) case as a baseline. Specifically, we vary T_0 from 0 to 5 using 51 uniformly spaced points. For each value of T_0, we carried out simulations across all homotypic interaction scenarios (HM1–HM4) and heterotypic scenarios (HT1–HT4), resulting in 204 simulations (for each case). We examined how $\max(u)$, the mean density $\langle u\rangle$ and the fraction of the spatial domain where

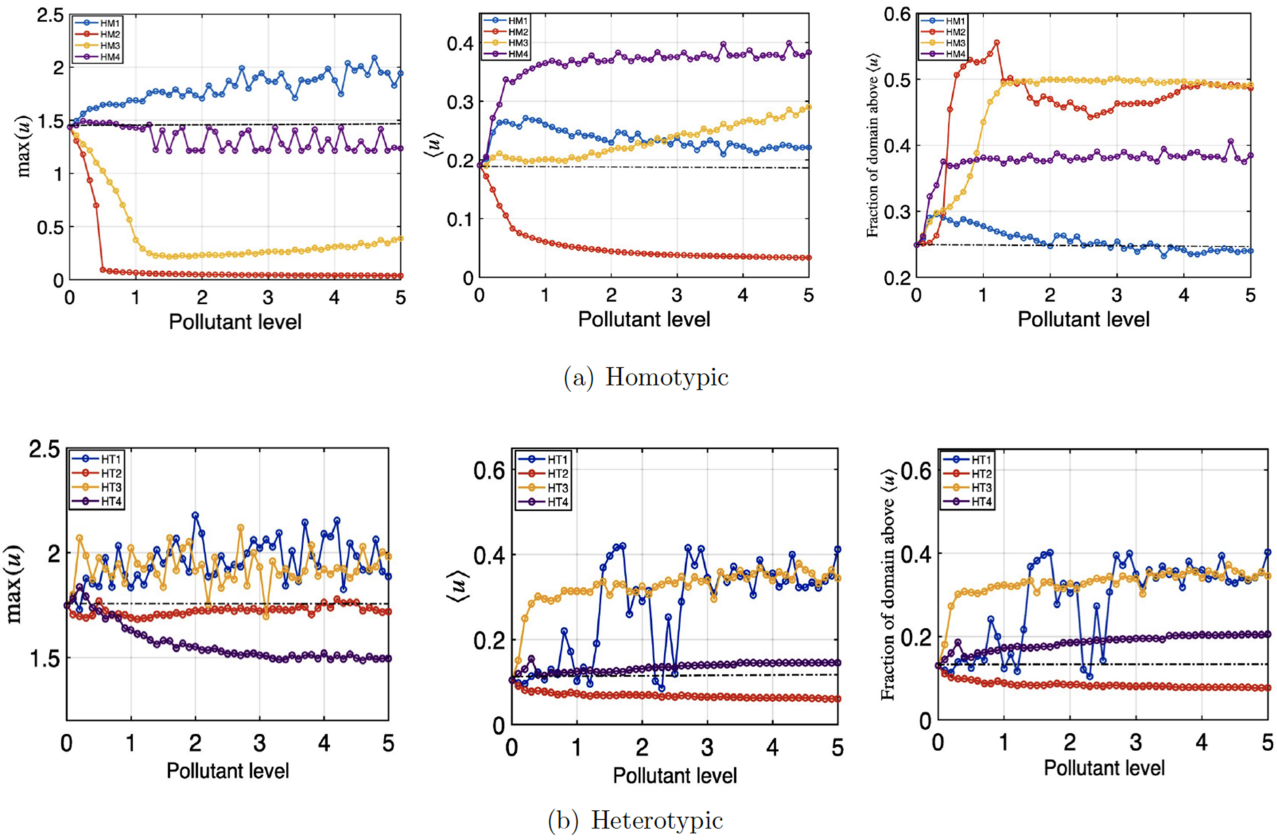

Figure 9. The effect of increasing pollutant levels on pigmentation, quantified by $\max(u)$, mean density $\langle u \rangle$ and the fraction of the domain where $u > \langle u \rangle$, for (a) homotypic interactions (HM1–HM4) and (b) heterotypic interactions (HT1–HT4). The dashed line denotes the baseline no-pollutant level for each metric. The parameters used in the simulation are $R_{vv} = 3$, $A_{uu} = 5$, $A_{vv} = 4$, $d_{uu} = 5$ and $d_{vv} = 3$. The pollutant field is defined as $T(i,j) = T_0\,(1 + 0.1\,\eta(i,j))$, with pollutant levels $T_0 \in [0, 5]$. Initial conditions are given by $u_0(i,j) = 1 + 0.01\,\xi_1(i,j)$ and $v_0(i,j) = 1 + 0.02\,\xi_2(i,j)$, where $\xi_k(i,j) \overset{\text{i.i.d.}}{\sim} \mathcal{N}(0,1)$.

melanophore density exceeds its mean value change with pollutant level. These measures provide a comprehensive assessment of pigmentation coverage and spatial organization.

Figure 9a summarizes how increasing pollutant intensity affects pigmentation levels and pattern characteristics under homotypic interactions (HM1–HM4). Under hypothesis HM2, both $\max(u)$ and $\langle u \rangle$ rapidly decline towards near-zero values, while the fraction of the domain above the mean remains nearly constant, indicating a loss of pigmentation corresponding to a no-pattern regime. In HM1, increasing pollutant levels lead to a slight increase in hyperpigmentation with mild fluctuations. In contrast, HM3 shows a monotonic increase in mean melanophore density with increasing pollutant levels, which approaches the $\max(u)$. Consequently, the value of $\max(u) - \langle u \rangle$ decreases, implying a loss of spatial heterogeneity (cf. supplementary material, figure S9). HM4 maintains a relatively high mean density with pronounced fluctuations in maximum melanophore density.

Figure 9b presents the response of heterotypic interactions (HT1–HT4) to increasing pollutant levels. Both HT2 and HT4 exhibit moderate fluctuations: HT2 shows a consistent decline in melanophore density, while HT4 shows a consistent rise. The simulated patterns under varying pollutant levels are shown in the supplementary material. In contrast, HT1 exhibits a high variance with rising pollutant levels, indicating high sensitivity towards increasing pollutants and enhanced spatial heterogeneity. As pollutant levels continue to rise, pigmentation changes, whether increasing or decreasing, do not intensify substantially beyond a critical threshold. In our simulations, this threshold occurs near $T_0 \approx 3$ (figure 9).

4.3. Short-time versus continuous exposure to pollutants

In this section, we examine how pattern formation and melanophore density change when fish experience pollutant exposure only during a short developmental stage, compared with continuous long-term exposure. We consider three treatment regimes: (i) a *short-stage exposure* treatment, in which pollution is applied during the early phase (time 0–150) and removed thereafter (time 150–300); (ii) a *continuous exposure* treatment, in which pollution is present throughout the entire simulation; and (iii) a *control* treatment with no pollutant at any time. Among all scenarios examined, the HM2 case exhibited the greatest loss of pigmentation in the homotypic setting. By contrast, for the heterotypic case, the pigmentation level did not show a significant difference between the short-stage and continuous exposure treatments. A full comparison of the three exposure regimes is presented in figure 10.

In the first treatment, the zebrafish is exposed to the pollutant only during a short-term window (until $t = 150$) and then transferred back to fresh water. At $t = 150$, we observe a faded spot pattern (cf. figure 10*a*), indicating that the pollutant has disrupted pattern maturation. The melanophore density is reduced, and the spatial pattern is less developed compared with

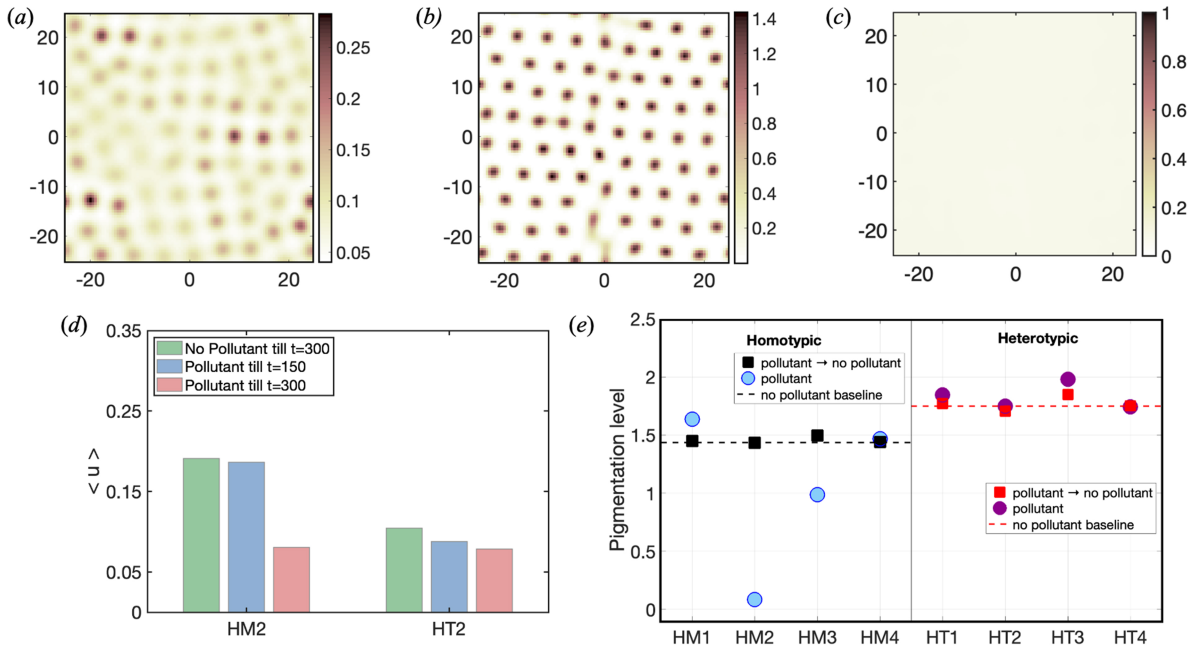

Figure 10. Simulation results showing the time-dependent effects of pollutant exposure. (*a*) Spatial pattern at $t = 150$ under pollutant exposure for HM2. (*b*) Partial recovery of the pattern at $t = 300$ after pollutant removal for HM2. (*c*) Strong suppression of pattern formation at $t = 300$ under continuous pollutant exposure for HM2. (*d*) Mean melanophore density $\langle u \rangle$ for HM2 and HT2 under three pollutant exposure regimes. (*e*) Summary of pigmentation changes in the homotypic and heterotypic cases. The pigmentation level is defined as the maximum melanophore density, $\max(u)$.

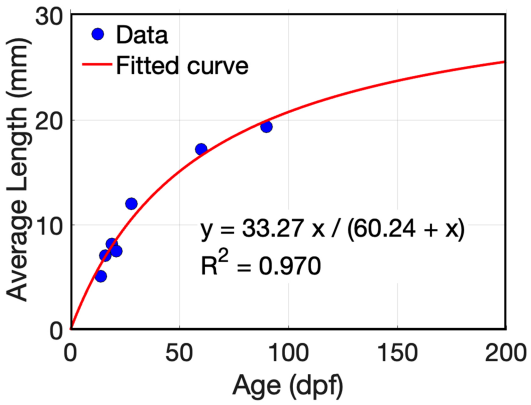

Figure 11. Fitted average domain length increase over age (data from [61]).

the control. After removal from the polluted environment, the system partially recovers (cf. figure 10*b*). The melanophore density increases and well-defined spots re-emerge; however, the maximum density remains slightly lower than in the control (cf. figure 10*d*). This suggests that short-term exposure can hinder normal pattern development, although partial recovery is possible once the environment improves. By contrast, when the zebrafish is exposed continuously from $t = 0$ to $t = 300$, we observe the strongest suppression of formation of the pattern (cf. figure 10*c*). Under both interaction mechanisms, HM2 and HT2, the model equation (2.1) produces the most severe hypopigmentation by $t = 300$ (cf. figure 10*d*). This indicates that continuous pollutant exposure exerts the greatest detrimental effect on pigment pattern formation. We summarize the results in figure 10*e*.

4.4. Hypo- and hyperpigmentation in pattern formation during fish development

To account for the effect of fish body growth on pattern formation, we consider a spatial domain that expands over time. As a motivating example, we focus on stripe formation during development. The average fish body length across ages is shown in figure 11 and is well approximated by the saturating function

$$y(t) = \frac{c\,t}{a + t},$$

with fitted parameters $c = 33.27$ and $a = 60.24$. This function captures a typical saturating growth law: body length increases rapidly during early development and gradually approaches a limiting size as the fish matures. In this work, fish growth is assumed to be independent of pollutant exposure. Growth data for fish larvae under methane exposure are provided in supplementary material, figure S3. In our experiments, growth measurements are available only up to $t = 4$ dpf, beyond which methane exposure becomes lethal and prevents further data collection. This modelling assumption allows us to isolate pollutant-induced changes in pigment cell interactions.

Let L_0 denote the initial characteristic length scale of the computational domain. We assume that the characteristic size of the growing domain is given by

$$L(t) = \frac{c\,(t + t_0)}{a + t + t_0},$$

where

$$t_0 = \frac{L_0 a}{c - L_0}$$

is chosen so that $L(0) = L_0$. Define the normalized growth factor

$$r(t) = \frac{L(t)}{L_0} = \frac{c\,(t + t_0)}{L_0(a + t + t_0)},$$

so that $r(0) = 1$. This defines a smooth isotropic expansion of the computational domain.

In one dimension, at any time t, we consider the domain $\Omega(t) = [-L(t), L(t)]$. In two dimensions, we consider $\Omega(t) = [-L(t), L(t)] \times [-L(t), L(t)]$. Mathematically, let $\hat{\Omega} \subset \mathbb{R}^n$ be a fixed reference domain. In the numerical simulations, we take the fixed reference domain to be $\hat{\Omega} = [-L_0, L_0]$ in one dimension and $\hat{\Omega} = [-L_0, L_0] \times [-L_0, L_0]$ in two dimensions. We describe isotropic growth through the mapping

$$\Gamma(\xi, t) = r(t)\xi, \qquad \xi \in \hat{\Omega},$$

which satisfies $\Gamma(\xi, 0) = \xi$. The growing spatial domain is therefore

$$\Omega(t) = \Gamma(\hat{\Omega}, t) = r(t)\hat{\Omega}.$$

The rescaled coordinate is defined by

$$\xi = \frac{x}{r(t)}, \qquad \xi \in \hat{\Omega},$$

which maps the evolving domain $\Omega(t)$ onto the fixed reference domain $\hat{\Omega}$. Under this change of variables, the governing equations on the growing domain are transformed to the following system on $\hat{\Omega}$:

$$\begin{aligned} u_t &= \frac{D_u}{r(t)^2}\Delta_\xi u - \frac{D_{uv}}{r(t)^2}\nabla_\xi \cdot \left(u\nabla_\xi(\widetilde{G}_{uv,r} * v)\right) - \frac{D_{uu}}{r(t)^2}\nabla_\xi \cdot \left(u\nabla_\xi(\widetilde{G}_{uu,r} * u)\right) + \chi(\xi, t) \cdot \nabla_\xi u + f(u, v), \\ v_t &= \frac{D_v}{r(t)^2}\Delta_\xi v - \frac{D_{vu}}{r(t)^2}\nabla_\xi \cdot \left(v\nabla_\xi(\widetilde{G}_{vu,r} * u)\right) - \frac{D_{vv}}{r(t)^2}\nabla_\xi \cdot \left(v\nabla_\xi(\widetilde{G}_{vv,r} * v)\right) + \chi(\xi, t) \cdot \nabla_\xi v + g(u, v), \end{aligned} \tag{4.2}$$

where

$$\chi(\xi, t) = \frac{\dot{r}(t)}{r(t)}\,\xi,$$

and $\dot{r}(t)$ denotes the time derivative of $r(t)$. The advection terms $\chi(\xi, t) \cdot \nabla_\xi u$ and $\chi(\xi, t) \cdot \nabla_\xi v$ account for the stretching induced by domain growth. Here, $\widetilde{G}_{uv,r}$, $\widetilde{G}_{uu,r}$, $\widetilde{G}_{vu,r}$ and $\widetilde{G}_{vv,r}$ denote the rescaled interaction kernels after the change of variables with $\widetilde{G}_{ij,r}(z) = r(t)^n G_{ij}(r(t)z)$. To model stripe continuation across the computational boundary, we impose periodic boundary conditions on the reference domain $\hat{\Omega}$. The detailed derivation can be found in the supplementary material.

As the domain expands, the spatial pattern also evolves: stripe spacing increases, and new stripes may emerge during growth. Figure 12 illustrates this behaviour in the absence of pollutant effects by showing representative two-dimensional snapshots at the developmental times 8, 34, 86, 182 and 251 dpf. Starting from an initial pattern consisting of one central stripe and two boundary stripes, additional stripes emerge progressively as the domain expands. At later times, pigmentation intensifies and the stripe boundaries become more sharply defined.

In the present model, we focus on pollutant-induced changes in pigment cell interactions during growth and neglect the direct effect of pollutants on domain growth. To examine these interaction-driven changes, we simulate the cases described in §4.1 with particular emphasis on perturbations of homotypic interactions (HM1–HM4). By excluding pollutant effects on body growth, we can better isolate and interpret the role of altered cell interactions in pattern formation. In the numerical examples below, we restrict attention to one- and two-dimensional spatial domains, which capture stripe-pattern dynamics while remaining computationally

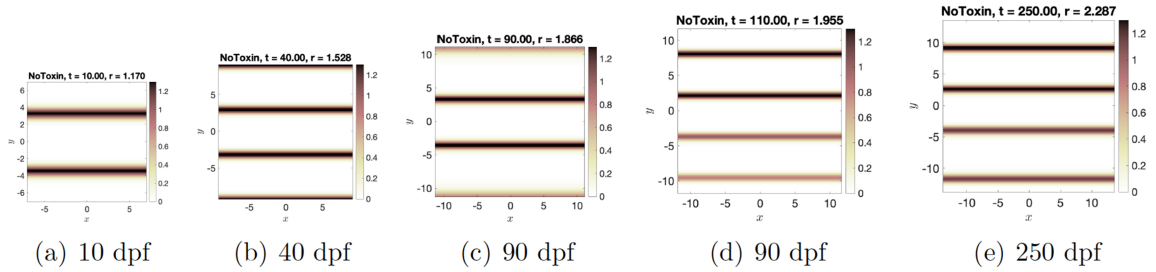

(a) 10 dpf (b) 40 dpf (c) 90 dpf (d) 90 dpf (e) 250 dpf

Figure 12. Simulation results showing pattern evolution during domain growth in the absence of pollutant effects. As the domain expands, the number of stripes increases. Parameters: $R_{vv} = 3, A_{uu} = 5, A_{vv} = 4, d_{uu} = 5, d_{vv} = 3, D_{uu} = D_{vv} = 0.8$ and growth law $L(t) = c(t + t_0)/(a + t + t_0)$.

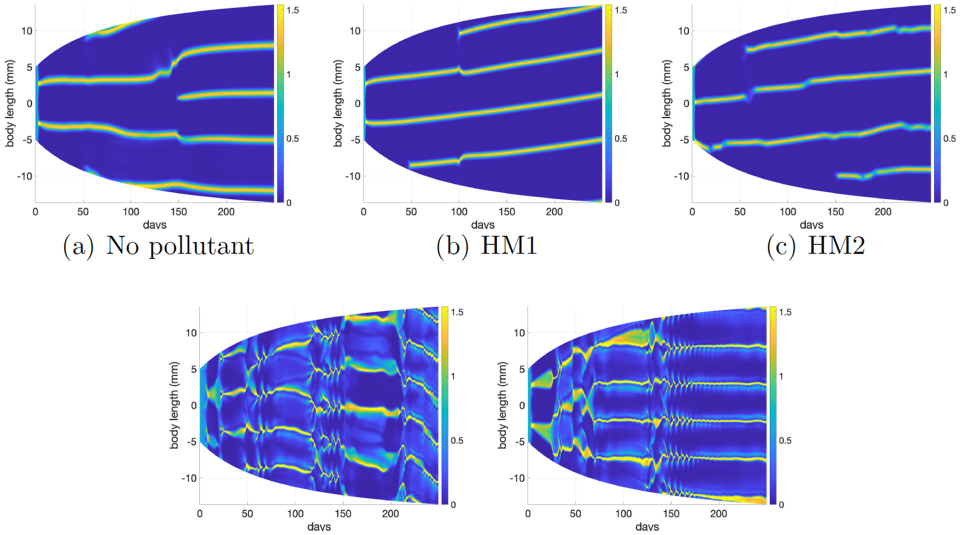

(a) No pollutant (b) HM1 (c) HM2

(d) HM3 (e) HM4

Figure 13. Comparison of observed and simulated pigment patterns during domain growth across the five hypotheses (no pollutant, HM1–HM4). Shown are representative stripe-formation processes during development. As the domain expands, additional stripes progressively emerge in both the experimental observations and the simulation results. Parameters: $R_{vv} = 3, A_{uu} = 5, A_{vv} = 4, d_{uu} = 5, d_{vv} = 3, D_{uu} = D_{vv} = 0.8$ and growth law $L(t) = c(t + t_0)/(a + t + t_0)$.

tractable. Since homotypic interactions are more sensitive to pollutant exposure, we focus on these cases to better understand pollutant effects during development. Figure 13 illustrates the temporal evolution of stripe patterns using a one-dimensional representation, making changes in stripe number, width, pigmentation intensity and formation speed easier to compare across hypotheses. Because the stripe pattern is relatively simple, the one-dimensional profile along a fixed cross-section captures the main qualitative features of the full two-dimensional pattern. Figure 12 complements this by showing representative two-dimensional snapshots at selected developmental stages.

Starting from an initial control pattern at $t = 0$, stripe addition continues as the domain grows; see figure 13a. When pollutant-induced alterations in cell–cell interactions are introduced, clear deviations from the control pattern emerge.

Under HM1, stripe formation exhibits the strongest developmental delay. The third stripe appears at approximately $t = 75$, substantially later than in the control case, where it forms around $t = 50$. By $t \approx 300$, the fourth stripe has only begun to emerge weakly, indicating the slowest stripe addition among all cases. These results suggest that HM1 significantly slows stripe development under pollutant exposure.

In the HM2 case, stripe structures persist throughout development but evolve more slowly than in the control. The third and fourth stripes appear at approximately $t = 70$ and $t = 270$, respectively, faster than in HM1 but still delayed relative to the control. In addition, the overall pigmentation intensity is markedly reduced, indicating sustained hypopigmentation.

For HM3 and HM4, the pigment pattern undergoes substantial changes during the early developmental stage ($t \lesssim 100$), corresponding to rapid transitions during the larval-to-adult period. At later times, the stripe patterns become more stable, with narrower stripes and clearer spatial organization for $t \gtrsim 200$. In both cases, stripe growth is accelerated relative to the control, and the third, fourth and fifth stripes appear earlier than in the control case. This accelerated stripe differentiation is clearly visible in figure 13d,e. Among the four scenarios, only HM2 produces a sustained reduction in pigmentation intensity.

5. Discussion

Developmental abnormalities induced by waterborne contaminants are widely used as biomarkers of aquatic ecosystem health [62]. In this study, we present a quantitative and mechanistic framework to investigate how environmentally relevant water pollutants affect pigment pattern formation in fish. Pattern development relies on the coordinated behaviour of pigment cells mediated by specific cellular interactions and morphogenetic processes [20]. For example, melanophores, xanthophores and iridophores interact to generate the characteristic black-and-yellow stripe pattern observed in wild-type fish [3,4,22].

Motivated by numerous pollutant-related empirical observations, we employed a non-local advection–diffusion model incorporating pollutant effects to investigate how altered pigment cell–cell interactions influence spatial patterning. Our results indicate that pollutant exposure not only alters overall pigmentation intensity, leading to hypo- or hyperpigmentation, but also reorganizes the spatial distribution of melanophores and xanthophores, resulting in increased pattern fragmentation and modified stripe configurations. These modelling predictions are consistent with our experimental findings: using ImageJ [49], we quantified pigment loss and disruptions in melanophore aggregation in methane-exposed fish, providing direct evidence of pollutant-induced hypopigmentation.

We extended the non-local reaction–diffusion–advection framework [3] to model interactions between melanophores and xanthophores in polluted environments. Polluted waters often contain complex mixtures of contaminants, including DIYA, fungicides, 2-amino-9H-pyrido[2,3-b]indol (AαC) and methane in oxygen-deficient conditions. Pollutant effects were modelled as modifications to adhesive and repulsive forces governing cell movement, incorporated through a interaction kernel that accounts for both short- and long-range interactions. Unlike classical diffusion, which assumes local random movement, the Morse-type kernel captures directed migration driven by attraction or repulsion over finite spatial ranges.

Numerical simulations revealed that pollutant-induced alterations in cell motility alone are sufficient to generate markedly different pigmentation patterns. Even without direct effects on reaction kinetics, changes in cell–cell interactions can fundamentally reshape pattern formation. Notably, pattern formation is more sensitive to homotypic modifications due to pollutant exposure than to heterotypic modifications.

By systematically varying adhesion and repulsion parameters, we reproduced spot-like mutant patterns and quantified how specific interaction changes produce hypo- or hyperpigmentation. For example, decreasing short-range repulsion while increasing melanophore adhesion (HM1) led to cell aggregation and reduced tissue-wide melanin coverage, producing pronounced hypopigmentation. By contrast, higher repulsion among pigment cells preserved spot structures, and certain combinations of adhesive–repulsive interactions among xanthophores generated stripes with higher melanin density. These findings identify the particular homotypic interactions that drive either darker or lighter pigmentation outcomes. For heterotypic interactions, keeping homotypic interactions unchanged while modifying only the melanophore–xanthophore interactions produced mixed spot–stripe patterns. Pigment loss was most pronounced under conditions of strong intercellular repulsion.

Our simulations also show that the timing and duration of pollutant exposure critically influence pigmentation outcomes. Short-term exposure delays pattern development, with partial recovery possible if conditions improve. By contrast, prolonged exposure results in severe hypopigmentation, for which recovery is minimal. Furthermore, we found that as pollutant levels increase, the overall effect generally becomes stronger; however, beyond a certain concentration, the effect saturates and does not intensify further. This phenomenon has been observed for specific pollutants, such as methane in our experiments, as well as AαC and 2,4-dinitrotoluene in previous studies [16]. Our results suggest that it may represent a more general effect of environmental pollutants on pigment pattern formation.

To capture developmental dynamics, we incorporated a growing domain representing fish body elongation. Using empirically fitted zebrafish growth curves, we simulated stripe formation on an expanding domain. Stripe addition continues during growth, but pollutant-induced changes in homotypic interactions alter the rate of stripe formation: HM1 and HM2 slow stripe addition at the early stage, whereas HM3 and HM4 accelerate it. This demonstrates that pollutant effects on cell–cell interactions can modulate both spatial patterning and temporal dynamics during development.

In summary, our work highlights the importance of understanding how pollutant-induced changes in short- and long-range cell–cell interactions shape pigment pattern formation. While direct experimental quantification of these interaction parameters remains challenging, our results provide a strong rationale for future experiments to investigate how contaminants modulate adhesive and repulsive forces between chromatophores. Such studies will be critical for precisely determining the underlying interaction mechanisms and for elucidating their role in driving pollutant-induced pigment pattern changes.

Ethics. This work did not require ethical approval from a human subject or animal welfare committee.

Data accessibility. The code supporting the findings is available at the Zenodo repository [63]. The data used during the study are included in the paper and in the supplementary material [64].

Declaration of AI use. We used ChatGPT (an AI language model) for minor assistance in language editing and phrasing. All scientific content, ideas and data were created and analysed by the authors.

Authors' contributions. P.R.C.: conceptualization, data curation, formal analysis, investigation, methodology, visualization, writing—original draft, writing—review and editing; T.X.W.: conceptualization, formal analysis, investigation, methodology, visualization, writing—original draft, writing—review and editing; A.M.: data curation; K.T.: conceptualization, funding acquisition, resources, supervision, writing—review and editing; H.W.: conceptualization, funding acquisition, methodology, project administration, supervision, validation, writing—review and editing.

All authors gave final approval for publication and agreed to be held accountable for the work performed therein.

Conflict of interest declaration. We declare we have no competing interests.

Funding. The research project was partially supported by an NSERC Alliance Missions grant on greenhouse gas research. The research of H.W. was partially supported by NSERC (Individual Discovery Grant RGPIN-2025-05734) and the CRC Program (Tier 1 Canada Research Chair). The research of K.T. was partially supported by NSERC (Individual Discovery Grant RGPIN-2021-02541).

Acknowledgements. This research was initiated while P.R.C. was affiliated with the University of Alberta. P.R.C also acknowledges the financial support of Axis Bank Centre for Mathematics and Computing to carry out part of this research work at the Department of Computational and Data Sciences, Indian Institute of Science, Bengaluru, India. We thank the anonymous reviewers for their constructive feedback and insightful suggestions, which significantly improved the quality of the manuscript.

References

1. Walderich B, Singh AP, Mahalwar P, Nüsslein-Volhard C. 2016 Homotypic cell competition regulates proliferation and tiling of zebrafish pigment cells during colour pattern formation. *Nat. Commun.* **7**, 11462. (doi:10.1038/ncomms11462)
2. Dawid IB. 2004 Developmental biology of zebrafish. *Ann. N.Y. Acad. Sci.* **1038**, 88–93. (doi:10.1196/annals.1315.015)
3. Volkening A, Sandstede B. 2015 Modelling stripe formation in zebrafish: an agent-based approach. *J. R. Soc. Interface* **12**, 20150812. (doi:10.1098/rsif.2015.0812)
4. Nakamasu A, Takahashi G, Kanbe A, Kondo S. 2009 Interactions between zebrafish pigment cells responsible for the generation of Turing patterns. *Proc. Natl Acad. Sci. USA* **106**, 8429–8434. (doi:10.1073/pnas.0808622106)
5. Martinson WD, Volkening A, Schmidtchen M, Venkataraman C, Carrillo JA. 2024 Linking discrete and continuous models of cell birth and migration. *R. Soc. Open Sci.* **11**, 232002. (doi:10.1098/rsos.232002)
6. Kondo S, Watanabe M, Miyazawa S. 2021 Studies of Turing pattern formation in zebrafish skin. *Phil. Trans. R. Soc. A* **379**, 20200274. (doi:10.1098/rsta.2020.0274)
7. Haffter P *et al*. 1996 Mutations affecting pigmentation and shape of the adult zebrafish. *Dev. Genes Evol.* **206**, 260–276. (doi:10.1007/s004270050051)
8. Jones ER, Bierkens MF, van Puijenbroek PJ, van Beek LRP, Wanders N, Sutanudjaja EH, van Vliet MT. 2023 Sub-Saharan Africa will increasingly become the dominant hotspot of surface water pollution. *Nat. Water* **1**, 602–613. (doi:10.1038/s44221-023-00105-5)
9. Bashir I, Lone FA, Bhat RA, Mir SA, Dar ZA, Dar SA. 2020 Concerns and threats of contamination on aquatic ecosystems. In *Bioremediation and biotechnology: sustainable approaches to pollution degradation*, pp. 1–26. Cham, Switzerland: Springer. (doi:10.1007/978-3-030-35691-0_1)
10. Haddeland I *et al*. 2014 Global water resources affected by human interventions and climate change. *Proc. Natl Acad. Sci. USA* **111**, 3251–3256. (doi:10.1073/pnas.1222475110)
11. Ejiohuo O, Onyeaka H, Akinsemolu A, Nwabor OF, Siyanbola KF, Tamasiga P, Al-Sharify ZT. 2024 Ensuring water purity: mitigating environmental risks and safeguarding human health. *Water Biol. Secur.* **4**, 100341.
12. Dong W, Yin X, Qi C, Wei T, Wei L, Yang J, Mu J, Teraoka H, Dong W. 2023 Reduced pigmentation and thyroid hormone disruption in zebrafish embryos caused by industrial sludge near Bohai Bay, China. *Water Biol. Secur.* **2**, 100190. (doi:10.1016/j.watbs.2023.100190)
13. Molagoda IMN *et al*. 2020 GSK-3β-targeting fisetin promotes melanogenesis in B16F10 melanoma cells and zebrafish larvae through β-catenin activation. *Int. J. Mol. Sci.* **21**, 312. (doi:10.3390/ijms21010312)
14. Karunarathne WAHM, Molagoda IMN, Kim MS, Choi YH, Oren M, Park EK, Kim GY. 2019 Flumequine-mediated upregulation of p38 MAPK and JNK results in melanogenesis in B16F10 cells and zebrafish larvae. *Biomolecules* **9**, 596. (doi:10.3390/biom9100596)
15. Kim YM, Lee EC, Lim HM, Seo YK. 2019 Rice bran ash mineral extract increases pigmentation through the *p*-ERK pathway in zebrafish (*Danio rerio*). *Int. J. Mol. Sci.* **20**, 2172. (doi:10.3390/ijms20092172)
16. Schmidt S, Busch W, Altenburger R, Küster E. 2016 Mixture toxicity of water contaminants-effect analysis using the zebrafish embryo assay (*Danio rerio*). *Chemosphere* **152**, 503–512. (doi:10.1016/j.chemosphere.2016.03.006)
17. Zhang T, Zhou XY, Ma XF, Liu JX. 2015 Mechanisms of cadmium-caused eye hypoplasia and hypopigmentation in zebrafish embryos. *Aquat. Toxicol.* **167**, 68–76. (doi:10.1016/j.aquatox.2015.07.021)
18. Peng L, Wang C, Li P, Cheng B, Hu Y, Cheng Y, Zheng Q. 2020 Evaluation of hypopigmentation in embryonic zebrafish induced by emerging disinfection byproduct, 3,5-di-I-tyrosylalanine. *Aquat. Toxicol.* **225**, 105525. (doi:10.1016/j.aquatox.2020.105525)
19. Mu X, Liu J, Yuan L, Huang Y, Qian L, Wang C. 2020 The pigmentation interference of bisphenol F and bisphenol A. *Environ. Pollut.* **266**, 115139. (doi:10.1016/j.envpol.2020.115139)
20. Patterson LB, Parichy DM. 2019 Zebrafish pigment pattern formation: insights into the development and evolution of adult form. *Annu. Rev. Genet.* **53**, 505–530. (doi:10.1146/annurev-genet-112618-043741)
21. Asai R, Taguchi E, Kume Y, Saito M, Kondo S. 1999 Zebrafish leopard gene as a component of the putative reaction-diffusion system. *Mech. Dev.* **89**, 87–92. (doi:10.1016/s0925-4773(99)00211-7)
22. Kondo S, Miura T. 2010 Reaction-diffusion model as a framework for understanding biological pattern formation. *Science* **329**, 1616–1620. (doi:10.1126/science.1179047)
23. Painter KJ, Maini PK, Othmer HG. 1999 Stripe formation in juvenile Pomacanthus explained by a generalized Turing mechanism with chemotaxis. *Proc. Natl Acad. Sci. USA* **96**, 5549–5554. (doi:10.1073/pnas.96.10.5549)
24. Yamaguchi M, Yoshimoto E, Kondo S. 2007 Pattern regulation in the stripe of zebrafish suggests an underlying dynamic and autonomous mechanism. *Proc. Natl Acad. Sci. USA* **104**, 4790–4793. (doi:10.1073/pnas.0607790104)
25. Watanabe M, Kondo S. 2015 Is pigment patterning in fish skin determined by the Turing mechanism? *Trends Genet.* **31**, 88–96. (doi:10.1016/j.tig.2014.11.005)
26. Maderspacher F, Nüsslein-Volhard C. 2003 Formation of the adult pigment pattern in zebrafish requires leopard and obelix dependent cell interactions. *Development* **130**, 3447–3457. (doi:10.1242/dev.00519)
27. Yamanaka H, Kondo S. 2014 In vitro analysis suggests that difference in cell movement during direct interaction can generate various pigment patterns in vivo. *Proc. Natl Acad. Sci. USA* **111**, 1867–1872. (doi:10.1073/pnas.1315416111)
28. Zhang C, Chen X, Wang J, Tan L. 2017 Toxic effects of microplastic on marine microalgae *Skeletonema costatum*: interactions between microplastic and algae. *Environ. Pollut.* **220**, 1282–1288. (doi:10.1016/j.envpol.2016.11.005)
29. Liu G, Jiang R, You J, Muir DC, Zeng EY. 2019 Microplastic impacts on microalgae growth: effects of size and humic acid. *Environ. Sci. Technol.* **54**, 1782–1789.

30. Izard T. 2025 Environmental toxicants and their disruption of integrin signaling in lipid rafts. *Bioessays* **47**, e202400276. (doi:10.1002/bies.202400276)
31. Huang W, Cao L, Ye Z, Lin L, Chen Q, Dou S. 2012 Tissue-specific bioaccumulation and oxidative stress responses in juvenile Japanese flounder (*Paralichthys olivaceus*) exposed to mercury. *Chin. J. Oceanol. Limnol.* **30**, 569–579. (doi:10.1007/s00343-012-1210-z)
32. Das BK, Roy S, Kumar V, Adhikari A, Ganguly S, Bisai K. 2025 Modulation of immune gene expression profile in *Labeo catla* with chronic toxicity to emerging endocrine disruptors through a multiorgan approach. *Sci. Rep.* **15**, 11244. (doi:10.1038/s41598-025-95996-7)
33. Turing AM. 1952 The chemical basis of morphogenesis. *Phil. Trans. R. Soc. Lond. B* **237**, 37–72. (doi:10.1098/rstb.1952.0012)
34. Painter KJ, Bloomfield J, Sherratt J, Gerisch A. 2015 A nonlocal model for contact attraction and repulsion in heterogeneous cell populations. *Bull. Math. Biol.* **77**, 1132–1165. (doi:10.1007/s11538-015-0080-x)
35. McGuirl MR, Volkening A, Sandstede B. 2020 Topological data analysis of zebrafish patterns. *Proc. Natl Acad. Sci. USA* **117**, 5113–5124. (doi:10.1073/pnas.1917763117)
36. Kondo S. 2012 Turing pattern formation without diffusion. In *Conference on computability in Europe*, pp. 416–421. Cham, Switzerland: Springer.
37. Bhaskar D, Zhang WY, Volkening A, Sandstede B, Wong IY. 2023 Topological data analysis of spatial patterning in heterogeneous cell populations: clustering and sorting with varying cell-cell adhesion. *NPJ Syst. Biol. Appl.* **9**, 43. (doi:10.1038/s41540-023-00302-8)
38. Giunta V, Hillen T, Lewis MA, Potts JR. 2025 A phylogeny of biological patterns formed by nonlocal advection. https://arxiv.org/abs/2506.00489.
39. Giunta V, Hillen T, Lewis MA, Potts JR. 2025 Positivity and global existence for nonlocal advection-diffusion models of interacting populations. *AIMS Math.* **10**, 21254–21272. (doi:10.3934/math.2025949)
40. Nakamasu AM. 2022 Correspondences between parameters in a reaction-diffusion model and connexin functions during zebrafish stripe formation. *Front. Phys.* **9**, 805659. (doi:10.3389/fphy.2021.805659)
41. Jewell TJ, Krause AL, Maini PK, Gaffney EA. 2025 Chase-and-run and chirality in nonlocal models of pattern formation. https://arxiv.org/abs/2505.17372.
42. Painter KJ, Giunta V, Potts JR, Bernardi S. 2024 Variations in non-local interaction range lead to emergent chase-and-run in heterogeneous populations. *J. R. Soc. Interface* **21**, 20240409. (doi:10.1098/rsif.2024.0409)
43. Singh AP, Nüsslein-Volhard C. 2015 Zebrafish stripes as a model for vertebrate colour pattern formation. *Curr. Biol.* **25**, R81–R92. (doi:10.1016/j.cub.2014.11.013)
44. Fang C, Di S, Zhang Y, Wang X, Jin Y. 2025 6PPD exposure reduced the melanin deposition by inhibiting tyrosinase activity in larval zebrafish. *Comp. Biochem. Physiol. C* **298**, 110300. (doi:10.1016/j.cbpc.2025.110300)
45. Moore MN. 1985 Cellular responses to pollutants. *Mar. Pollut. Bull.* **16**, 134–139.
46. Manzano-Covarrubias AL, Yan H, Luu MD, Gadjdjoe PS, Dolga AM, Schmidt M. 2023 Unravelling the signaling power of pollutants. *Trends Pharmacol. Sci.* **44**, 917–933. (doi:10.1016/j.tips.2023.09.002)
47. Nikinmaa M. 1992 How does environmental pollution affect red cell function in fish? *Aquat. Toxicol.* **22**, 227–238. (doi:10.1016/0166-445X(92)90042-L)
48. Roberts DW, Costello JF. 2003 Mechanisms of action for general and polar narcosis: a difference in dimension. *QSAR Comb. Sci.* **22**, 226–233. (doi:10.1002/qsar.200390016)
49. Schneider CA, Rasband WS, Eliceiri KW. 2012 NIH image to ImageJ: 25 years of image analysis. *Nat. Methods* **9**, 671–675. (doi:10.1038/nmeth.2089)
50. Cornell RA, Yemm E, Bonde G, Li W, d'Alençon C, Wegman L, Eisen J, Zahs A. 2004 Touchtone promotes survival of embryonic melanophores in zebrafish. *Mech. Dev.* **121**, 1365–1376. (doi:10.1016/j.mod.2004.06.005)
51. Parichy DM. 2021 Evolution of pigment cells and patterns: recent insights from teleost fishes. *Curr. Opin. Genet. Dev.* **69**, 88–96. (doi:10.1016/j.gde.2021.02.006)
52. Budi EH, Patterson LB, Parichy DM. 2008 Embryonic requirements for ErbB signaling in neural crest development and adult pigment pattern formation. *Development* **135**, 2603–2614. (doi:10.1242/dev.019299)
53. Quigley IK, Parichy DM. 2002 Pigment pattern formation in zebrafish: a model for developmental genetics and the evolution of form. *Microsc. Res. Tech.* **58**, 442–455. (doi:10.1002/jemt.10162)
54. Wang C, Xu J, Kocher TD, Li M, Wang D. 2022 CRISPR knockouts of pmela and pmelb engineered a golden tilapia by regulating relative pigment cell abundance. *J. Hered.* **113**, 398–413. (doi:10.1093/jhered/esac018)
55. Cavalieri V, Spinelli G. 2017 Environmental epigenetics in zebrafish. *Epigenet. Chromatin* **10**, 46. (doi:10.1186/s13072-017-0154-0)
56. Fairbairn EA, Bonthius J, Cherr GN. 2012 Polycyclic aromatic hydrocarbons and dibutyl phthalate disrupt dorsal–ventral axis determination via the Wnt/β-catenin signaling pathway in zebrafish embryos. *Aquat. Toxicol.* **124**, 188–196. (doi:10.1016/j.aquatox.2012.08.017)
57. Wormley DD, Ramesh A, Hood DB. 2004 Environmental contaminant mixture effects on CNS development, plasticity, and behavior. *Toxicol. Appl. Pharmacol.* **197**, 49–65. (doi:10.1016/j.taap.2004.01.016)
58. Zhou W, Wang Y, Wang J, Peng C, Wang Z, Qin H, Li G, Li D. 2022 β-Ionone causes endocrine disruption, hyperpigmentation and hypoactivity in zebrafish early life stages. *Sci. Total Environ.* **834**, 155433. (doi:10.1016/j.scitotenv.2022.155433)
59. Hayazaki M, Hatano O, Shimabayashi S, Akiyama T, Takemori H, Hamamoto A. 2021 Zebrafish as a new model for rhododendrol-induced leukoderma. *Pigment Cell Melanoma Res.* **34**, 1029–1038. (doi:10.1111/pcmr.13005)
60. Owen J, Kelsh R, Yates C. 2020 A quantitative modelling approach to zebrafish pigment pattern formation. *eLife* **9**, e52998. (doi:10.7554/eLife.52998)
61. Wallace CK, Bright LA, Marx JO, Andersen RP, Mullins MC, Carty AJ. 2018 Effectiveness of rapid cooling as a method of euthanasia for young zebrafish (*Danio rerio*). *J. Am. Assoc. Lab. Anim. Sci.* **57**, 58–63.
62. Mubashshir M, Ovais M. 2026 Melanophore: a biosensor for water pollution analysis. *Biochimie* **241**, 16–25.
63. Roy Chowdhury P. 2026 Codes: Pollutant-induced changes in fish pigmentation and spatial patterns [Data set]. Zenodo. (doi:10.5281/zenodo.19553954)
64. Roy Chowdhury P, Wang T, MacDonald A, Tierney K, Wang H. 2026 Supplementary material from: Pollutant-induced changes in fish pigmentation and spatial patterns. Figshare. (doi:10.6084/m9.figshare.c.8561734)